Surface & Coatings Technology 474 (2023) 130094

Contents lists available at ScienceDirect

Surface & Coatings Technology

journal homepage: www.elsevier.com/locate/surfcoat

Full Length Article

Enhanced electroless Ni-P plating quality on binderless tungsten carbide by atmospheric pressure plasma pretreatment

Weijia Guo [a,1], Muneeb Khan [a,1], Tianfeng Zhou [a,b,*], Yupeng He [a], Yongjie Zhang [c,d], Peng Liu [a,b], Bin Zhao [a], Qian Yu [a], Xibin Wang [a], Hui Deng [c]

[a] Department of Mechanical Engineering, Beijing Institute of Technology, Beijing 300081, China
[b] Beijing Institute of Technology Chongqing Innovation Center, Chongqing 401120, China
[c] Department of Mechanical and Energy Engineering, Southern University of Science and Technology, Shenzhen 518055, Guangdong, China
[d] Department of Physics, National University of Singapore, Singapore 117551, Singapore

ARTICLE INFO

Keywords:
AP plasma pretreatment
Binderless WC mold
Electroless Ni—P plating

ABSTRACT

Precision glass molding (PGM) has been widely utilized in optical components production, during which binderless tungsten carbide (WC) is a popular mold material. Researchers have proposed the application of electroless nickel-phosphorus (Ni—P) plating on WC molds, offering good surface finish, non-stick properties, and enhanced corrosion resistance, while typical Ni—P plating pretreatment is complex, time-consuming, carrying risks of surface damage and pollution. In this study, Atmospheric-pressure (AP) plasma surface processing has been proposed as an alternative pretreatment technique to enhance electroless Ni—P plating quality on binderless WC, contributing to the reduction of plating steps, time, smoothing of the plated Ni—P layer, and improvement in adhesion quality. The interaction mechanism between AP plasma and WC has been analyzed. The influence of AP plasma surface pretreatment on the surface quality of Ni—P plating has been investigated in detail. Surface characterization and adhesion test have been conducted to evaluate the effectiveness of AP plasma pretreatment method. Despite the fact the replication of substrate roughness exists in typical Ni—P plating process, the surface roughening and enhanced surface energy induced by AP plasma pretreatment can have a smoothing effect for the following electroless Ni—P plating process. The effectiveness of ICP AP plasma as an alternative pretreatment technique for high-quality electroless Ni—P plating on binderless WC has been validated.

1. Introduction

Precision glass molding has been widely utilized in the production of lenses, prisms, mirrors, and other optical components in industries, including aerospace, defense, medical, and telecommunications etc. [1–3]. This process involves heating a glass preform to its softening temperature and then pressing it into a mold to create the desired shape, during which the choice of mold material is critical for achieving the high accuracy and good surface quality of the produced glass components [4]. Commonly used mold materials for PGM molds include tungsten carbide (WC), silicon carbide (SiC), and other ceramics, which possess properties such as high hardness, good thermal stability, high wear resistance, non-stick properties, and high thermal conductivity. Binderless WC is popular in PGM, due to its excellent combination of hardness, wear resistance, and thermal stability. It can withstand the high temperature and pressure without degradation or deformation during the PGM process. The excellent wear resistance ensures that the mold can retain its shape and dimensions over time, which is crucial for high volume production. In addition, binderless WC has a low coefficient of thermal expansion, which guarantees the mold dimensions and shape, resulting in an accurate and repeatable production [5–7]. What's more, the excellent thermal conductivity enables quick heat transfer during the molding process, which remains the correct temperature and consistency throughout the molding process and contribute to a high-quality finished product with uniform optical properties. However, limitations still exist. For example, the high hardness of binderless WC makes it difficult to be machined, which can have a rough surface and lead to the surface defects of the glass component during the molding process. It is also possible that the glass preform would stick to the mold surface, resulting in damage during the demolding process. The WC mold is

* Corresponding author at: Beijing Institute of Technology Chongqing Innovation Center, Chongqing 401120, China.
E-mail address: zhoutf@bit.edu.cn (T. Zhou).
[1] The two authors contribute equally to this paper.

https://doi.org/10.1016/j.surfcoat.2023.130094
Received 4 September 2023; Received in revised form 27 September 2023; Accepted 10 October 2023
Available online 11 October 2023

susceptible to corrosion as well, which can cause its degradation or failure [8].

To address the above-mentioned problems, researchers proposed the application of electroless nickel-phosphorus (Ni—P) plating on WC molds, so that to improve the mold performance and promise the quality of the glass component. Ni—P plating offers good surface finish, non-stick properties, reduced friction, and enhanced corrosion resistance of WC molds. These benefits can help produce high-quality glass components with greater efficiency and lower costs. It was in 1946 that Brenner and Riddel successfully developed formulations and experiments on electroless Ni-Plating. Gould et al. studied the kinetics of electroless Ni—P plating [9]. It was found that the platings exhibit excellent anti-wear property, good corrosion resistance and machinability [10,11]. Jafari et al. applied Ni—P plating to improve the wear resistance of WC cutting tools, making them suitable for high-speed machining and other demanding applications. The effect of electroless Ni—P platings on the performance of WC cutting tools has been explored [12]. Di Egidio et al. evaluated the influence of Ni—P plating as an interlayer between diamond-like carbon plating and WC substrates. The authors found that the Ni—P plating can significantly improve the adhesion strength of the platings, contributing to an improved wear resistance and durability [13]. Overall, it has been proved that Ni—P plating is an effective surface treatment method for improving the performance of WC in various applications, by the enhancement of wear resistance, adhesion strength, corrosion resistance, and tribological properties of WC, enabling its usage in harsh environments.

Typical electroless Ni—P plating on WC involves cleaning and surface preparation, activation, electroless Ni—P plating, post treatment and finishing process [14]. It has been proved that the electroless Ni—P plating can provide a uniform, conformal plating surface with good adhesion and corrosion resistance. Careful control of the electroless plating process and post-treatment steps are important to ensure proper adhesion and performance of the plating. To promise the quality of Ni—P plating, several pretreatment methods have been taken, such as surface cleaning, surface activation, surface roughening, degreasing and tailoring of plating composition with addition of nanoparticles [15–17]. Although these methods can be effective, they still have some limitations or disadvantages. It has been found that etching or roughening may create micro-cracks, defects, or residual stresses that may reduce the mechanical strength or durability of the substrate, and further cause the risk of surface damage or degradation, which can limit the practical applications of the coated WC parts, especially in high-stress or corrosive environments [18,19]. Surface activation using palladium catalysts requires careful control of the catalyst deposition and activation steps to avoid excessive oxidation or contamination. Pre-treatment solutions may also involve hazardous or toxic chemicals that require careful handling and disposal, which is not environmentally friendly either [20]. The addition of inorganic non-metal nanoparticles, such as Si, SiC, ZnO and Al_2O_3 etc. have been conducted by researcher, although the mechanical properties and corrosion resistance of the nano-composite coatings is superior. These methods are being phased out due to their possible high cost or harmful effects. Controlled addition of inorganic nanoparticles, without poison and contamination, to the treatment bath has become a good alternative [21–24]. Future study is needed to be conducted to optimize the pretreatment methods and develop new approaches that can overcome these limitations and enable broader applications of coated WC parts.

Atmospheric-pressure (AP) plasma surface pretreatment method therefore has been proposed in this study to enhance the performance of Ni—P plating on WC, during which the plasma will be exposed to the WC substrate. It is a non-contact surface modification method that the WC mold surface can be effectively activated and cleaned, without introducing any damage or defect. This method is also more environmentally friendly and efficient, making it a potential alternative for Ni—P plating pretreatment in PGM applications. The interaction mechanism between AP plasma and WC has been analyzed. The influence of AP plasma surface pretreatment on the surface quality of Ni—P plating has been investigated in detail. Surface characterization has been conducted to evaluate the effectiveness of AP plasma pretreatment method. Adhesion test has been performed to validate the improvement in bonding strength between Ni—P plating and WC substate, with the pretreatment by AP plasma.

2. Materials and methods

2.1. Material preparation

In this study, WC with two types of surface configuration have been utilized for comparison. The cylindrical binderless WC workpieces were supplied by Chaofeng Micro-Nano Technology (Ningbo) Co., Ltd., with diameter of 20 mm and thickness of 5 mm. The theoretical density per centimeter is 15.4 g/cm^2. The photograph and surface microscope image are shown as in Fig. 1. The rough binderless WC surface was cut from a long rod through diamond wire saw, of which the surface roughness is measured to be an average of Ra ~ 3.6 μm. It is taken as the first type of workpiece surface configuration and shown with fully distributed saw marks, as shown in Fig. 1(a). While the polished surface was taken as the second type of surface configuration and it is achieved through Chemical Mechanical Polishing (CMP) using silicon carbide abrasive paper with grit sizes of 400, 800, and 1000 in sequence. When switching to different grits of sandpaper, the polishing direction was changed by 90°, allowing the distinct shadowy traces left by the previous grit to be easily identified. Additionally, diamond polishing agent was employed in the process. As a result, the polished surface exhibited an average roughness of Ra ~ 100 nm, as shown in Fig. 1(b).

2.2. AP plasma pretreatment

Fig. 2 shows the optical photograph and schematic diagram of the AP plasma pretreatment experimental setup. Inductively coupled plasma (ICP) has been utilized. The experimental arrangement for AP plasma surface pretreatment on WC workpiece is illustrated. The setup comprises several components, including RF power supply (40.68 MHz), a copper inductor coil, a quartz torch tube, an alumina ceramic sample table, and a three-axis Computerized Numerical Control (CNC) motion system. The quartz torch tube (ID: 20 mm) is positioned at the center of the induction coil and consists of two coaxial quartz tubes. The inner tube is responsible for supplying ignition gas (Ar, 1.5 slm) and reaction gas (O_2, 20 sccm), while the outer tube provides cooling gas (Ar, 18 slm) to prevent the fused quartz torch tube from melting under high temperatures. The distance between plasma torch and WC workpiece is fixed at 20 mm. Additionally, this arrangement stabilizes the ICP plasma beam. During the pretreatment, WC workpiece will be irradiated by the ICP plasma and can undergo a comprehensive and precise surface treatment, by employing the CNC motion platform. The experimental details have been listed as in Table 1.

2.3. Electroless Ni—P plating process

The electroless Ni—P plating process was carried out using a wire activation system. The required chemicals and process flow are listed in Table 2. As the substrate cannot be directly employed for electroless Ni—P plating due to the presence of various impurities resulting from previous machining processes, a sequence of pre-treatment steps is necessary to be conducted prior to the electroless Ni—P plating process, involving ethanol cleaning, degreasing, and acid picking, so that to eliminate contaminants, during which the following chemical reactions happen:

Degreasing:

$$2NaOH + Na_2O_3 + Na_2PO_4 + H_2O \rightarrow 2Na_3PO_4 + CO_2 + H_2O \quad (1)$$

Acid Picking:

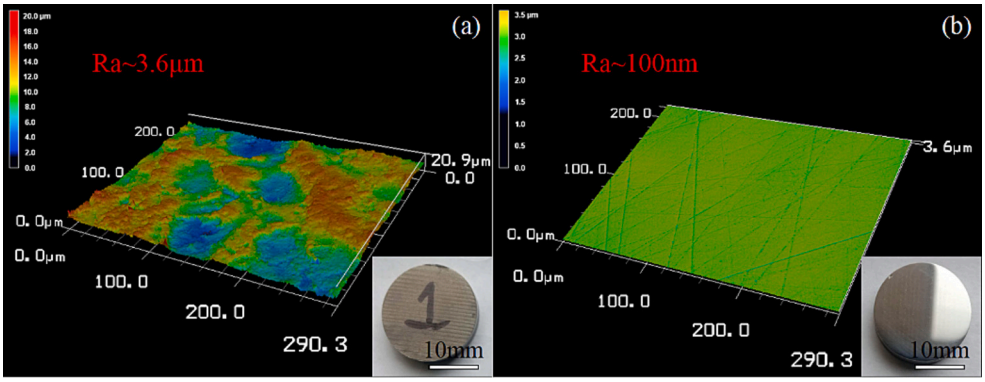

Fig. 1. The photograph and 3D surface microscope image: (a) sawing sample surface (Ra ~ 3.6 μm); (b) polishing sample surface (Ra ~ 100 nm).

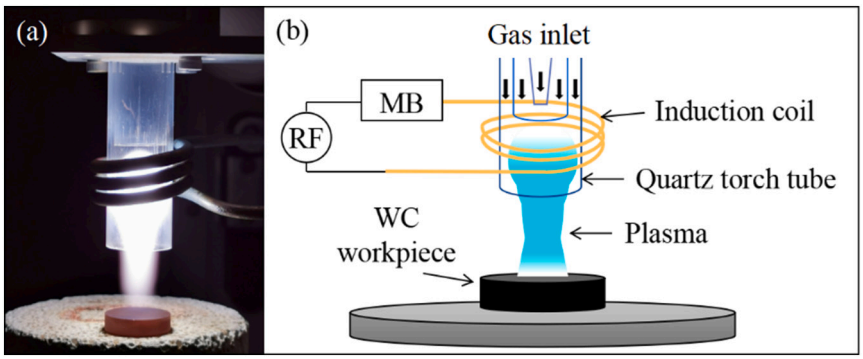

Fig. 2. AP plasma experimental setup: (a) optical photograph; (b) schematic diagram.

Table 1
Experimental parameters for AP plasma pretreatment.

Parameters	Values
RF power (W)	800
Ignition gas (slm)	1.5
Cooling gas (slm)	18
Reaction gas (sccm)	20
Substrate-torch distance (mm)	20
Plasma duration (min)	1, 5, 10, 15

$$HCl + H_2O \rightarrow H_3O^+ + Cl^- \quad (2)$$

Electroless Ni—P Plating:

$$2Ni^{2+} + H_2PO^{2-} + 3H_2O \rightarrow 2NiP + 4H^+ + 2HPO_4{}^{2-} \quad (3)$$

The cleaning solutions used for surface preparation Ethanol, degreasing (NaOH, Na_2CO_3, Na_2PO_4) and acid picking (HCl) were of analytical grade and met the required purity standards from Fuchen (Tianjin) Chemical Reagent Co, Ltd. and the electroless Ni—P plating solution employed was from Shenzhen Fushuntai Technology Co., Ltd., with a purity level of 99 %.

As depicted in Fig. 3, the pre-treatment procedure, including ethanol cleaning, degreasing, and acid picking, were conducted at a water bath temperature of 60 °C, with durations of 30, 15, and 15 min, respectively, aiming at activating the substrate and facilitating a strong interfacial bond with the plating materials. In between each step, the substrate was rinsed with deionized water for 2 min to eliminate the residuals from the previous solution.

During the degreasing step, as outlined by Eq. (1), a combination of chemicals including 7.5 g/L sodium hydroxide (NaOH), 35 g/L sodium carbonate (Na_2CO_3), 15 g/L sodium phosphate (Na_2PO_4), and water (H_2O) were used. These agents collaborated to effectively remove grease and other contaminants from the substrate's surface. NaOH, acting as a potent base, was responsible for the breakdown of organic residues, while Na_2CO_3 and Na_2PO_4 potentially contributed to the emulsification or breakdown of grease.

The acid picking process, as expressed by Eq. (2), employed a 60 mL

Table 2
Process flow of electroless Ni—P plating on WC substrate.

Step	Process	Solution composition		Condition
1	Ultrasonic Cleaning	Ethanol	100 mL	30 min, 20 °C
2	Washing	DI water	100 mL	5 min, 60 °C
3	Degreasing	Sodium Hydroxide (NaOH)	7.5 g/L	15 min, 60 °C
		Sodium Carbonate (Na_2CO_3)	35 g/L	
		Tri-Sodium Phosphate (Na_2PO_4)	15 g/L	
4	Cleaning	DI water	100 mL	2 min, 60 °C
5	Acid Picking	HCL	10 vol%	15 min, 60 °C
		DI water	90Vol%	
6	Cleaning	DI water	100 mL	2 min, 60 °C
7	Electroless plating	Nickel Sulfate $NiSO_4.7H_2O$	30 g/L	5-6 h, 85 °C water bath
		Sodium Hypophosphite $NaH_2PO_2.H_2O$	20 g/L	
		Lactic acid $CH_3CH(OH)COOH$	25 g/L	
		Propionic Acid CH_3CH_2COOH	5 g/L	
		Thiourea (CH_4N_2S) or Lead (Pb^{2+})	0.001 g/Lor 0.003 g/L	
		Loading capacity	1.5dm^2/L	
		pH	4.7	
8	Cleaning	DI water	100 mL	5 min, 60 °C

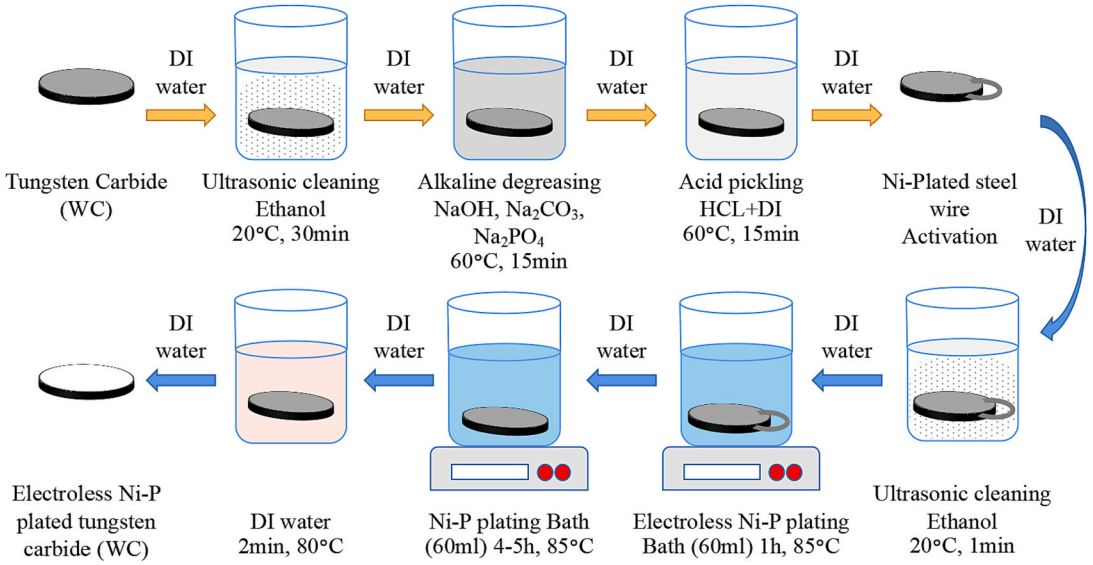

Fig. 3. Schematic diagram of the electroless Ni—P plating process using wire activation system.

solution consisting of 10 % hydrochloric acid (HCl) and 90 % water (H_2O). This solution effectively removed oxides, scale, and impurities from the substrate's surface through acid dissolution, thereby revealing the underlying matrix structure of the substrate.

Lactic acid ($C_3H_6O_3$) was added to the solution to prevent undesired side reactions, maintain plating bath stability, control deposition rate, enhance the quality of the plated layer, and minimize the formation of phosphate precipitates ($NiHPO_3$). Furthermore, propionic acid (CH_3CH_2COOH) acted as a buffering agent to stabilize the pH throughout the plating process, with the pH ranging from 4 to 6, and an optimal pH of 4.7 achieved using ammonium hydroxide ($NH_3{\cdot}H_2O$). Thiourea (CH_4N_2S) was incorporated into the solution to prevent the decomposition of the reducing agent and maintain the desired plating characteristics.

To enhance the bonding strength between the substrate and plating, a clean Ni-plated steel wire was utilized to facilitate the rapid deposition of a thin Ni layer onto the substrate surface. When the Ni-plated steel wire contacted the substrate surface, the substrate acted as the cathode, while the Ni—P solution functioned as the anode, initiating the reduction reaction. Within 30 min, a thin layer of Ni would be formed, covering the substrate surface. Subsequently, the Ni-plated steel wire was removed, and the electroless plating process proceeded to coat the entire surface. The complete plating process typically lasted around 5–6 h, conducted within an 85 °C water bath. Following the plating step, the Ni—P plated WC substrate underwent a cleaning process using DI water heated to 60 °C, after which it was allowed to cool down to room temperature.

Overall, the typical Ni—P plating process is a time-consuming process and involves several complex steps, especially the surface pretreatment steps, which lead to the longer overall time consumption. While AP plasma surface pretreatment can contribute to the reduction of plating steps, time, and is proposed as an alternative pretreatment technique to enhance electroless Ni-P plating quality on binderless WC.

2.4. Characterization and measurement

Before the experiments, all the WC workpieces have been ultrasonically cleaned with deionized (DI) water and ethanol. The free radical composition of AP plasma has been characterized by an optical emission spectrometer (OES, Ocean Optics USB4000) with a wavelength resolution of 0.2 nm. The surface morphology and topography have been observed using 3D laser confocal scanning microscopy (LCSM, VK-X1000, Keyence, Japan) and field-emission scanning electron microscope (SEM, S-4800, Hitachi, Japan) with an acceleration voltage of 15 kV. The surface roughness has also been measured using LCSM. Energy dispersive spectrometer (EDS) was used to test the elemental composition of treated surface. The Vickers hardness were tested using digital microhardness tester (HXD-1000, Shanghai Taiming Optical Instrument Co., Ltd., China) with a diamond pyramidal indenter. Five points on the plating surface were tested at various stages: before plasma treatment, after plasma treatment. The tests were conducted under two different load conditions, including 50 g and 100 g. The Water contact angle (WCA) was obtained by a contact angle measuring instrument (OCA25, Dataphysics, Germany), so that to evaluate the surface energy. The thickness of the oxide film after plasma pretreatment were measured by multi-wavelength ellipsometer (FS-1, Film Sense, USA). The adhesion quality has been evaluated by performing Rockwell-C indentation test, with a durometer WIZHARD HR-522 (Mitutoyo, Kanagawa, Japan) under the load of 60 N. The morphology of trace edges has been observed using SEM, so that to evaluate the bonding strength between the Ni—P plating and WC substrate, according to the VDI standard 3198. The microstructure of the Ni—P platings through typical electroless Ni—P plating process on sawing substrate and polished substrate and AP plasma enhanced Ni—P plating on polished substrates have been characterized by X-Ray diffractometer (XRD, D8 ADVANCE, Bruker AXS, Germany) using Cu-Kα radiation ($\lambda = 1.54$ Å). The diffraction scanning scope ranged from 5° to 90° with a step of 0.02° at a scanning rate of 5 s/step. The average grain size was calculated by the Debye-Scherrer formula by applying the phase identifying software (MDI Jade 6, Gatan, USA).

3. Results and discussion

3.1. AP plasma pretreatment surface characterization

The composition of free radicals in ICP plasma was characterized by OES spectrum, as shown in Fig. 4, generated with RF power set at 800 W. The optical fibre probe was positioned at a fixed distance of approximately 200 mm from the center of the torch. To ensure consistency, a constant integration time of 60 ms was used for recording the emission spectrum of all collected data. In the spectrum, the wavelength of each emission line corresponds to a specific element, while the emission intensity indicates the number density of free radicals present. Distinctive peaks corresponding to argon emission can be detected. The atomic

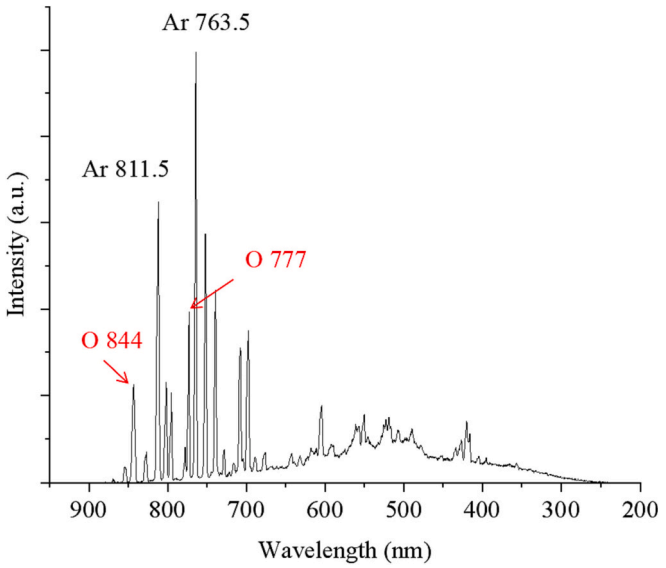

Fig. 4. OES spectrum of the ICP plasma (800 W).

oxygen peaks at 777 nm and 844 nm represent the transitions O (3p5P → 3s5S) and O (3p3P → 3s3S), respectively [25]. The OES result illustrates that the AP plasma contains O radicals that may oxidized the WC surface.

In addition to the plasma diagnose, the elemental composition of the samples was also evaluated to provide a comprehensive understanding of the oxide formation. As shown in Fig. 5, obvious peaks can be observed on the AP plasma processed surface, the weight percentage and atomic percentage show a great increase, compared to the sample before AP plasma processing, of which only W element and C element dominate on the surface. Based on the analysis above, the AP plasma may result in the oxidation of WC surface with various forms of oxide [26]. The chemical reaction is as follows:

$$2WC + 10O \rightarrow 2WO_3 + CO_2 \quad (5)$$

The oxide thickness was determined by measuring the average value at five different locations on each sample. The measured thickness values were 10.559 nm, 18.733 nm, and 30.840 nm for plasma processing durations of 1 min, 5 min, and 10 min, respectively. However, after 15 min of plasma processing, the surface became excessively rough, making it challenging to accurately measure the oxide thickness, as shown in Fig. 6(a). The surface roughness is measured to be Ra ~ 130 nm, 480 nm, 685 nm and 805 nm, respectively, as shown in Fig. 6.

Fig. 7 shows the surface morphology of WC after plasma procession duration of 1 min. The surface is observed with irregular shapes and clusters of white dots, connecting with each other, which could potentially be oxide formations, due to the preferential oxidation along the grain boundaries, as enlarged in Fig. 7(b). It is noteworthy that the same phenomenon can be observed along selective scratches, as shown in Fig. 7(c) and enlarged in Fig. 7(d).

While a unique surface morphology can be observed after a plasma processing duration of 5 min, as shown in Fig. 8(a) and enlarged in Fig. 8 (b). The formation of wormlike surface appearance can be observed, attributed to the diffusion of oxygen radical and the reaction kinetics. It is generally believed that the wormlike morphology arises from the anisotropic nature of the reaction. The reaction proceeds more readily along certain crystallographic directions, leading to the preferential growth of oxide protrusions in specific directions.

Based on the above observation, during ICP plasma processing, locally preferential oxidation can occur, and the grain boundaries and scratches tend to be oxidized first. Grain boundaries and scratches provide sites of increased reactivity compared to the bulk material. These regions often have higher energy and a greater density of defects, such as: dangling bonds or broken atomic bonds, which can facilitate the adsorption of reactive species and lead to oxidation. It is also possible that grain boundaries and scratches are more likely to accumulate surface contaminants, such as organic residues or adsorbed atmospheric species. These contaminants can act as initiators for oxidation reactions by facilitating the formation of reactive species or providing reaction sites. As a result, the presence of contaminants at grain boundaries and scratches can enhance the rate of oxidation in these regions. In addition, during the ICP plasma processing, a high-frequency electric field is applied to the plasma. This electric field can induce localized electric field effects near grain boundaries and scratches. These electric field effects can lead to the generation of reactive species, such as oxygen radicals, through processes like electron impact dissociation. The increased concentration of reactive species near grain boundaries and scratches promotes their preferential oxidation. The presence of stress can induce localized stress concentrations and alter the local chemical potential, making these regions more prone to oxidation. Stress can promote the breaking of existing atomic bonds and provide additional energy for oxidation reactions to occur. It is important to note that anisotropic oxidation behavior can exhibit under certain experimental parameters (5 min), which is more pronounced in binderless WC due to the absence of a metallic binder phase. The lack of a binder phase may expose more of the WC surface and influence the oxidation kinetics on specific crystallographic planes. In addition, binderless WC retains the hexagonal crystal structure with a c-axis perpendicular to the basal plane. The (0001) basal plane of WC, which consists of alternating layers of tungsten and carbon atoms, is typically more reactive and susceptible

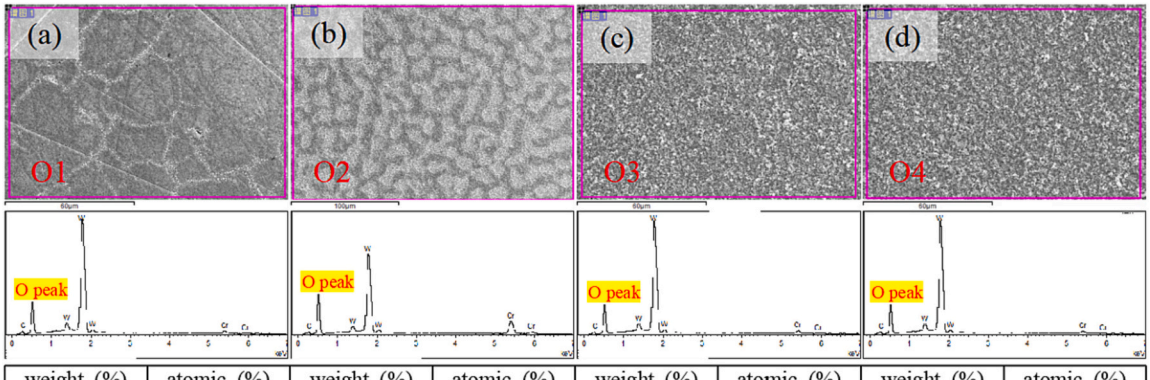

weight (%)	atomic (%)	weight (%)	atomic (%)	weight (%)	atomic (%)	weight (%)	atomic (%)
21.66	66.52	25.47	66.47	21.53	74.42	20.98	66.81

Fig. 5. EDS results of WC sample after AP plasma pretreatment processing: (a) pretreatment duration of 1 min (denoted as O1); (b) pretreatment duration of 5 min (denoted as O2); (c) pretreatment duration of 10 min (denoted as O3); (d) pretreatment duration of 15 min (denoted as O4).

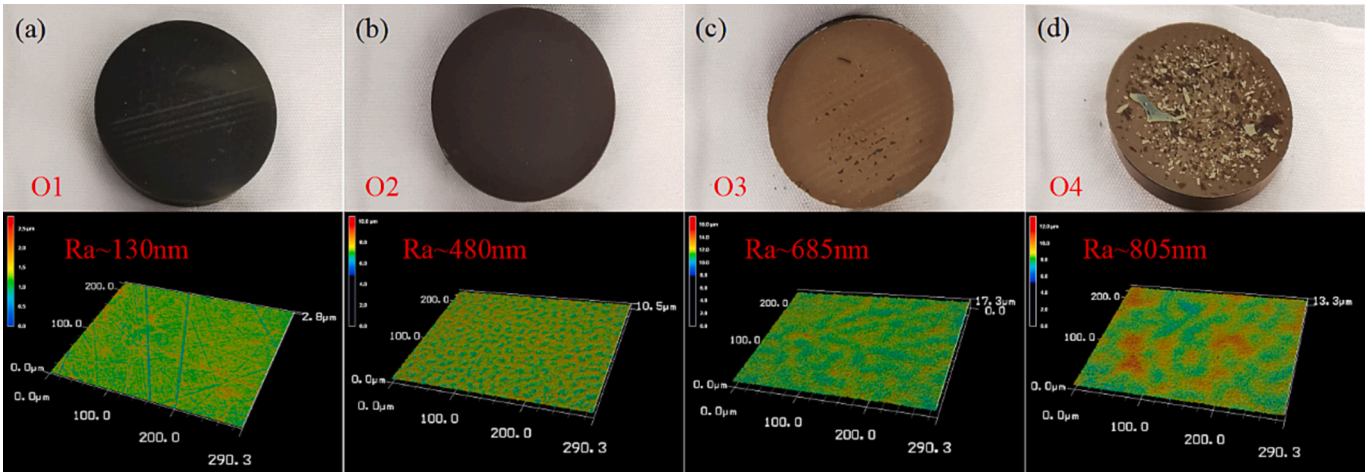

Fig. 6. Photograph and 3D laser confocal scanning microscope surface image of WC sample after AP plasma pretreatment processing: (a) pretreatment duration of 1 min (O1); (b) pretreatment duration of 5 min (O2); (c) pretreatment duration of 10 min (O3); (d) pretreatment duration of 15 min (O4).

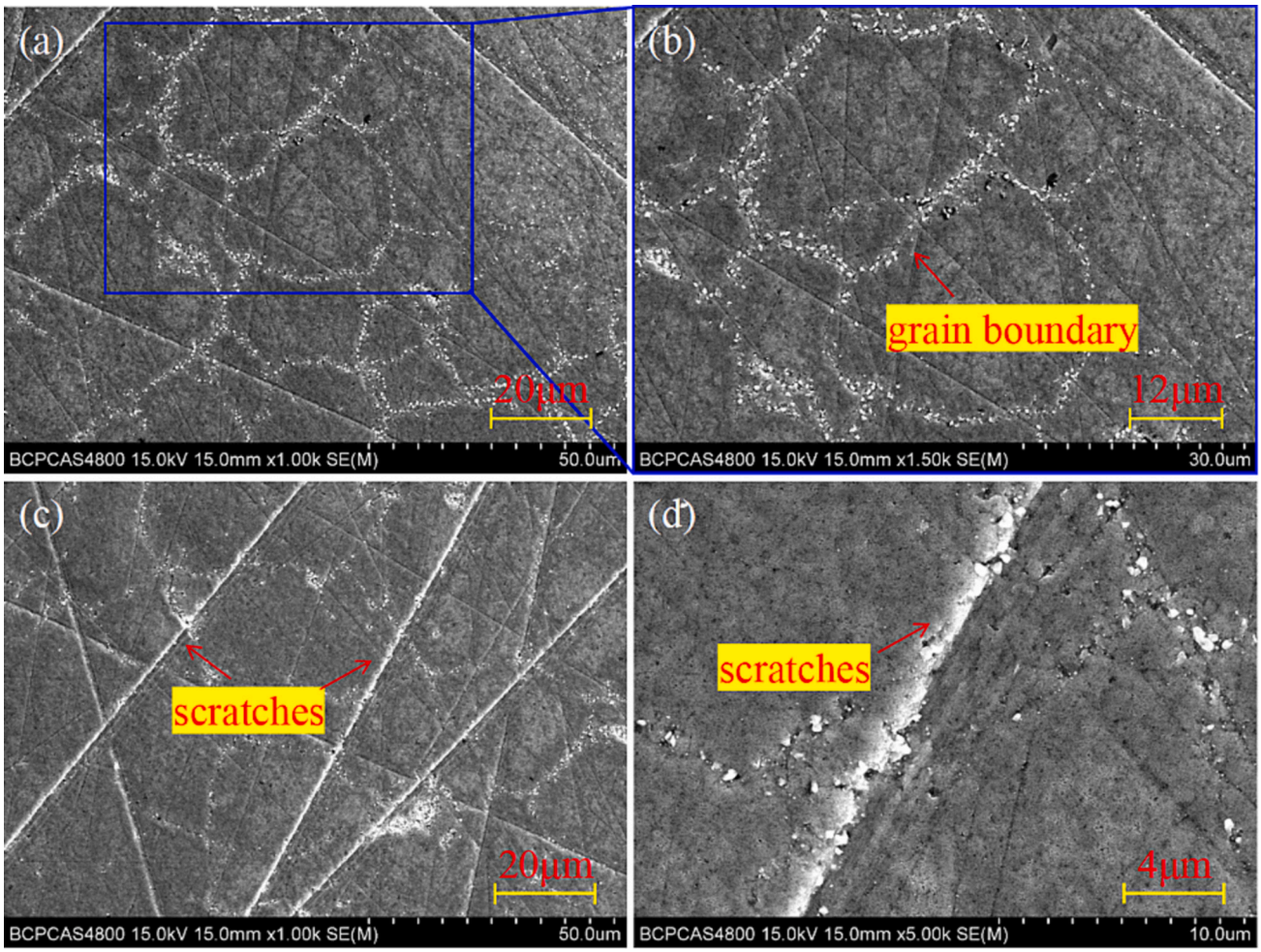

Fig. 7. SEM image of the plasma processed WC surface (1 min): (a) overall appearance; (b) enlarged local area grain boundary; (c) appearance of scratch; (d) enlarged local scratch.

to oxidation compared to other crystallographic planes. This could be attributed to the grain orientation. Anisotropic oxidation can happen when the grains preferentially oriented in a specific direction. The crystallographic planes exposed on the surface of each grain will determine their reactivity towards the plasma environment.

As the oxidation progresses over an extended period (10 min and 15 min), the oxide layer can become more uniform, and the differences in reactivity between crystallographic planes might become less pronounced, as shown in Fig. 8(c) and (d). This can lead to the more isotropic oxidation behavior, where the growth of wormlike structures

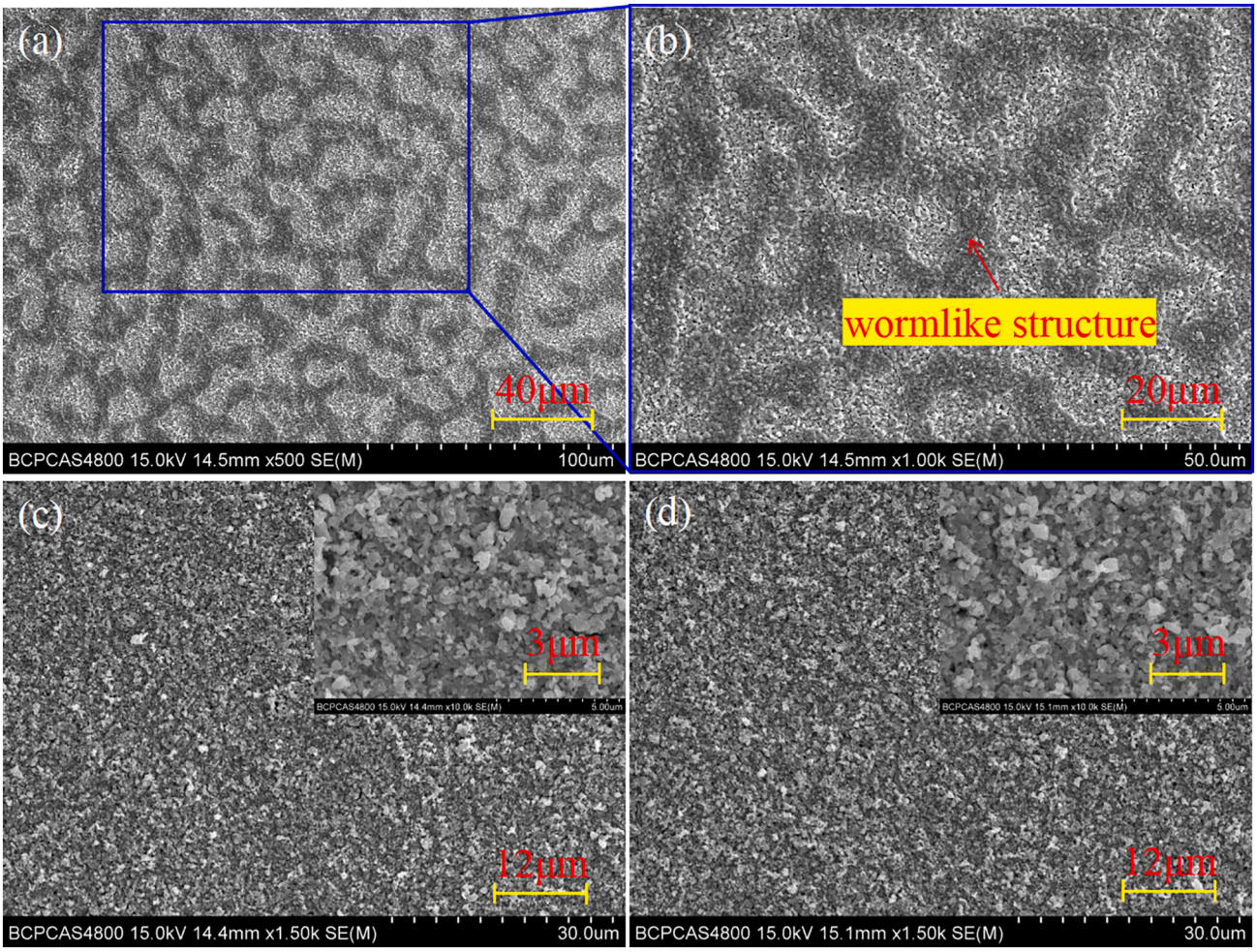

Fig. 8. SEM image of the plasma processed WC surface: (a) 5 min; (b) enlarged local area of 5 min; (c) 10 min; (d) 15 min.

or preferential oxide protrusions along specific crystallographic directions becomes less prominent.

The Vickers hardness (HV) has been measured to be reduced after AP plasma pretreatment, as is shown in Fig. 9. The surface hardness measurements were performed on samples subjected to different durations of AP plasma surface modification. After AP plasma surface modification, the average surface hardness of O1 (1min), O2 (5min), O3 (10min), O4 (15min) and standard deviation (represented by the error bars) have been measured to be 301.0 HV, 263.5 HV, 171.7 HV and 195.5 HV respectively, which indicates a clear decrease in surface hardness, with longer treatment durations generally leading to greater reductions in hardness, compared to the original hardness of 3060.3 HV.

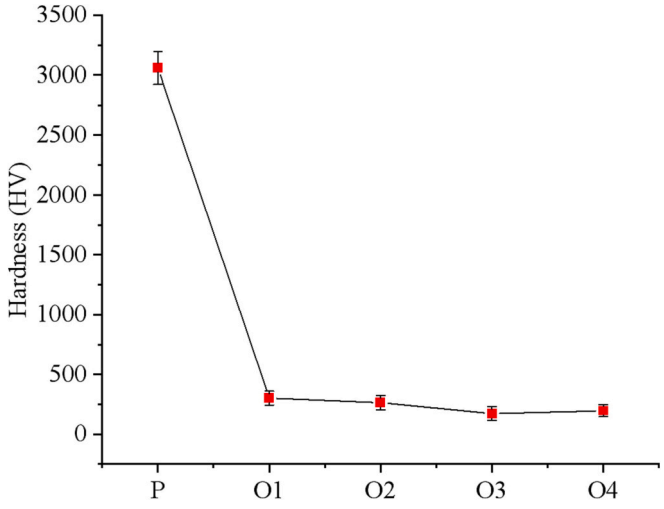

Fig. 9. Hardness measurement result (P: Polished surface, O1: plasma processing duration of 1 min, O2: plasma processing duration of 5 min, O3: plasma processing duration of 10 min, O4: plasma processing duration of 15 min).

To evaluate the surface energy change after the AP plasm pretreatment, the WCA has been measured for the original samples and AP plasma surface modified samples, as shown in Fig. 10. It has been observed that the WCA can be reduced from 90.75° to 72.8°, after the self-polishing process, due to the decrease of the effective surface area after polishing. After the AP plasma surface treatment, it is shown that there is a greater reduction in WCA from 72.8° to 38.6°. The surface energy of WC has been increased, making it more receptive to the wetting and spreading of the Ni—P plating solution. The improved wetting ability may ensure a uniform plating process and reduction of the chances for defects on plating surfaces.

To summarize, AP plasma surface pretreatment can induce surface roughening on WC. The roughened surface can provide an increased surface area for the Ni—P plating to adhere to, improving mechanical interlocking between the WC and the plating, which can enhance overall durability and wear resistance [27]; In addition, plasma treatment can introduce active species such as ions, radicals, and reactive species. This activation enhances the surface energy and promotes chemical bonding between the WC and the Ni—P plating. The improved bonding can lead to better adhesion and reduced chances of plating delamination. The

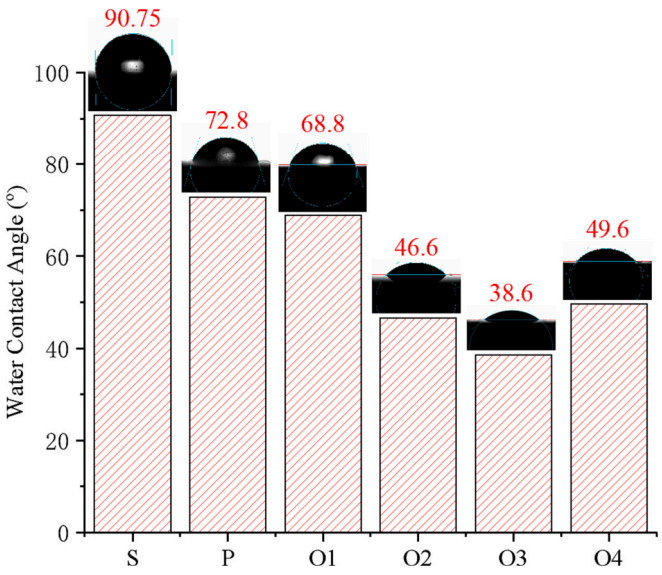

Fig. 10. Water contact angle results (S: sawing sample, P: polishing sample, O1: plasma processing duration of 1 min, O2: plasma processing duration of 5 min, O3: plasma processing duration of 10 min, O4: plasma processing duration of 15 min).

increased surface energy also makes it more receptive to the spreading of the Ni—P plating solution. This improved wettability ensures uniform plating thickness and can reduce the chances of defects; Furthermore, AP plasma surface pretreatment can effectively clean the WC surface, removing contaminants and organic compounds. It can eliminate the need for additional cleaning steps, such as degreasing or acid etching, which can rapidly realize the pretreatment, contributing to the reduction of overall required plating steps and time. Experimental trials and characterization techniques have been employed to determine the effectiveness of AP plasma on Ni—P plating on WC surface and validate the improvement in adhesion and bonding strength.

3.2. Typical electroless Ni—P plating surface characterization

The surface morphology of the plating on both polishing surfaces and sawing surfaces before heat treatment have been characterized by SEM, as shown in Fig. 11. Despite the locally continuous and smooth appearance, as shown in Fig. 11(a), nodules and rounded protuberances can be formed on the surface, as shown in Fig. 11(b), and enlarged in Fig. 11(c). Closely spaced cellular structures can be observed on the plating, as shown in Fig. 11(d). Irregular shapes arise as well on the surface and the grain-like structure can be enlarged as in Fig. 11(f).

Based on the above surface morphology analysis, during the electroless plating process, the formation of the Ni—P plating occurs through nucleation and subsequent growth of particles on the substrate surface. These particles can initially appear as spherical nodules. Nodules and rounded protuberances can form on a surface as nucleation site, which may arise from the deposition of impurities, localized variations in material composition, or the accumulation of particles during the processing. In the early stages of plating, the individual spherical particles may not have had sufficient time or conditions for coalescence or merging. They may remain as discrete spherical entities on the plated surface. As the plating progresses, the particles that form on the substrate surface can tend to agglomerate or cluster together due to van der Waals force or electrostatic interactions. This agglomeration can result in the formation of spherical particle clusters.

Although the surface morphology of the Ni—P plating on the sawing WC is shown with less nodules and more of cellular and grain-like structure on the surface. The incomplete plating coverage can be observed, as shown in Fig. 12. Since nodules typically form during the plating process due to various factors such as impurities, localized variations, or uneven deposition. It tends to form in areas with a high deposition rate or where the plating bath has limited access, leading to localized growth. The sawing WC surface would result in a non-uniform deposition, meaning that there may be areas of lower deposition and therefore fewer spherical nodules can be observed. In addition, the sawing WC surface is rough and characterized by irregularities, such as peaks, valleys, and surface asperities, which would hinder the formation of well-defined spherical nodules. They may give rise to a more complex

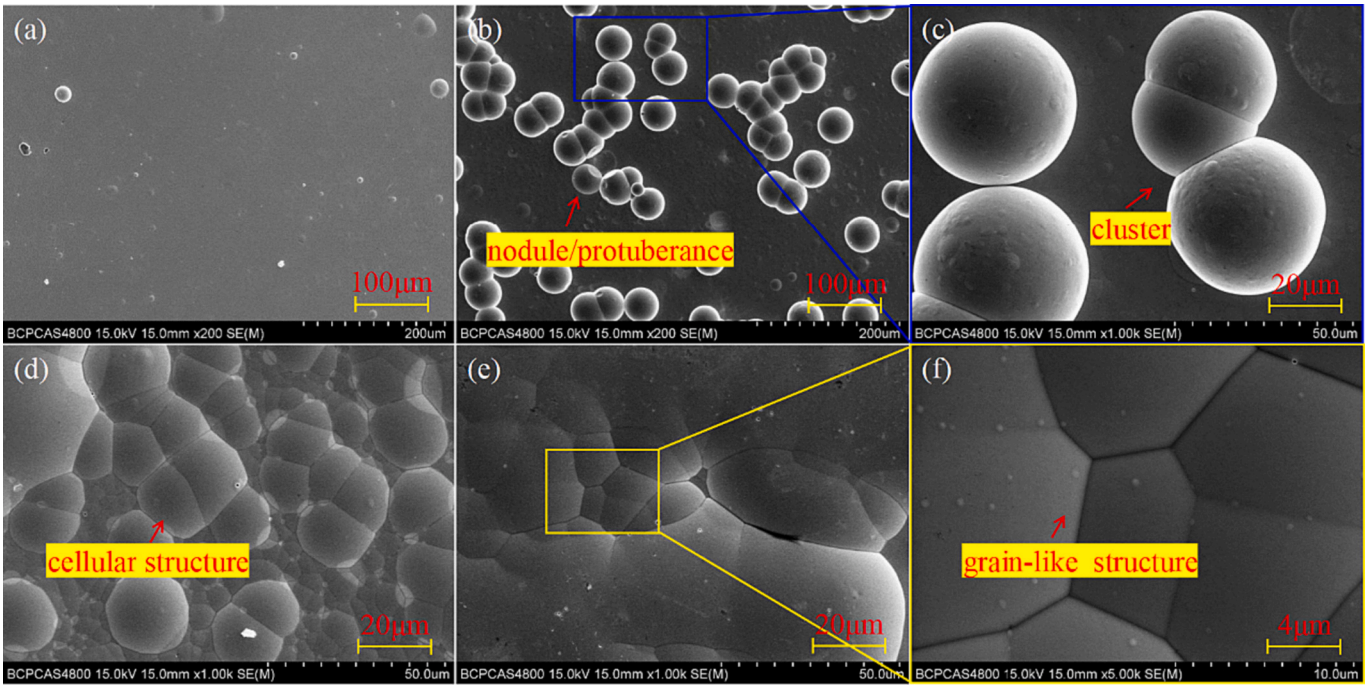

Fig. 11. SEM image of Ni—P plating surface on WC (polishing): (a) locally smooth area; (b) nodules; (c) enlarged nodules; (d) cellular structure; (e) locally irregular area; (f) enlarged grain-like structure.

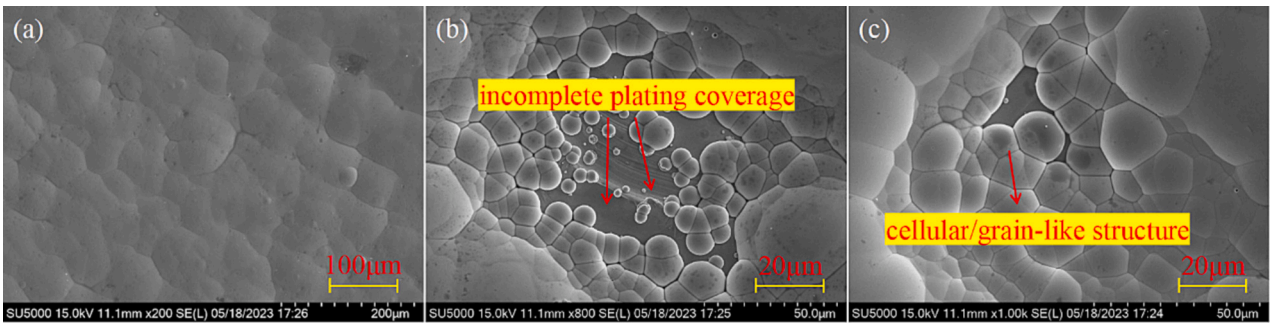

Fig. 12. SEM image of Ni—P plating surface on WC (sawing sample): (a) locally smooth area; (b) incomplete plating coverage area; (c) cellular structure and grain-like structure.

surface morphology with a mixture of irregular shapes and structures. At the same time, the surface irregularities provide localized areas with different surface orientations and growth conditions. The uneven deposition rates associated with a rough surface can lead to variations in crystal growth, resulting in the development of distinct grain boundaries and grain-like structures. What's more, the non-uniform deposition and uneven distribution of plating material can lead to variations in plating thickness and coverage, resulting in areas with inadequate deposition, which can give rise to defects such as voids and incomplete plating coverage, as shown in Fig. 12(b).

Along with the EDS results, the plating is shown consisting of Ni and P elements and belongs to the high phosphorus electroless Ni—P plating, as shown in Fig. 13. The phosphorus content of the as plated Ni—P surface through typical electroless Ni—P plating method is tested to be 12.88 % (locally smooth area) and 13.85 % (spherical nodule), respectively.

3.3. AP plasma enhanced electroless Ni—P plating surface characterization

To avoid the incomplete plating coverage and non-uniform surface caused by surface roughening, the polishing sample has been taken to examine the effectiveness of AP plasma surface enhancement of electroless Ni—P plating on WC mold. The surface characteristics are shown in Section 3.1, after which the Ni—P plating has been performed on the surface. The surface morphology of WC after AP plasma enhanced electroless Ni—P plating for a duration of 1 min (denoted as O1P) is depicted in Fig. 14. It is shown that almost no spherical nodules and rounded protuberances can be observed on the surface. The Ni—P plating exhibit uniform deposition. AP plasma pretreatment can effectively remove contaminants and organic compounds from the WC surface. By eliminating potential sources of particle contamination, plasma treatment can help reduce the occurrence of surface nodules when conducting Ni—P plating. The improved surface energy by AP plasma activation creates a more receptive surface for the subsequent Ni—P plating, contributing to a uniform deposition and potentially reducing the irregular formation of rounded nodules and surface defects. The increased surface roughness after AP plasma treatment can promote mechanical interlocking between the substrate and the Ni—P plating and provide a more stable plating environment, minimizing the likelihood of surface irregularities.

However, the rough surface can lead to the trapping of air and leave gas bubble on the Ni—P plating, as shown in Fig. 14(a). Despite this, the gas bubbles are smaller than 6 μm of diameter and tend to be hollow voids within the plating, which may not significantly affect the Ni—P plating adhesion and integrity. While the elemental composition does not show discrepancy, compared with typical Ni—P plating method without AP plasma pretreatment, 13.22 % (weight percentage) of phosphorous has been obtained. The surface morphology of WC after AP plasma enhanced electroless Ni—P plating for a duration of 5 min (denoted as O2P), duration of 10 min (denoted as O3P) and duration of 15 min (denoted as O4P) are depicted in Fig. 15. Despite the increased surface roughness from O1 to O4, the Ni—P plating surface looks smooth and uniform, seldom gas bubbles can be observed, while locally contamination exists.

The surface roughness and surface topography of the Ni—P plated surface are depicted in Figs. 16 and 17, respectively. The results clearly demonstrate a significant reduction in surface roughness after electroless Ni—P plating. The initial surface roughness of the sawing surface was measured at Ra ~ 3.6 μm. However, after plating, although the surface is not entirely uniform, the surface roughness shows a considerable improvement, reaching Ra ~ 404 nm. This reduction in surface roughness indicates a substantial enhancement in surface quality. Furthermore, after self-polishing, the surface roughness experienced a further improvement, measuring at Ra ~ 100 nm. Based on this enhanced starting point, the subsequent Ni—P plating process leads to a remarkable reduction in surface roughness, reaching Ra ~ 75 nm. This signifies a refinement in the surface quality of the Ni—P plated surface.

In addition, the surface roughness of the AP plasma pretreated surface demonstrates an increasing trend with longer AP plasma treatment. However, after Ni—P plating, the surface roughness shows a significant reduction compared to Ni—P plating on both sawing and polishing

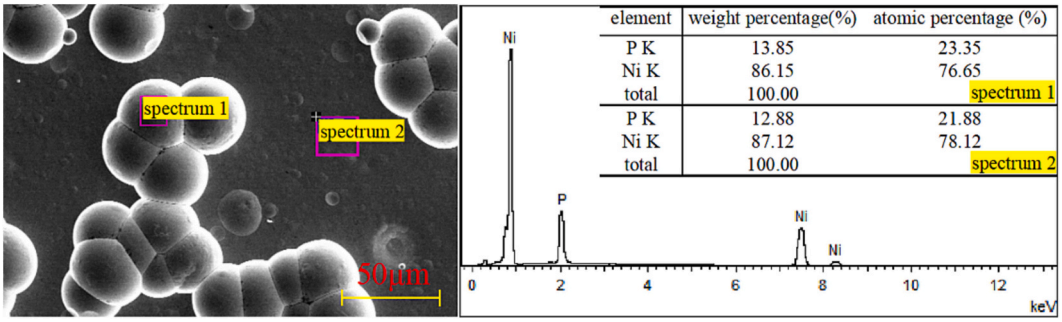

Fig. 13. EDS of Ni—P plating on WC (polishing): spectrum 1 of the spherical nodule; spectrum 2 of the locally smooth area.

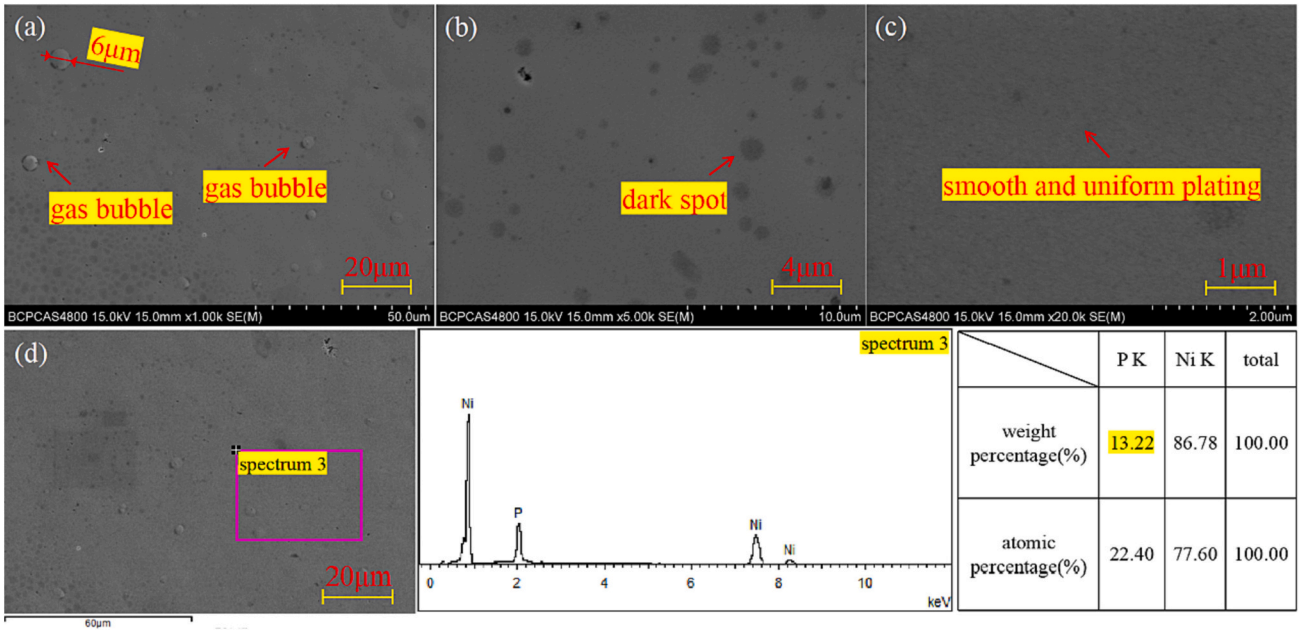

	P K	Ni K	total
weight percentage(%)	13.22	86.78	100.00
atomic percentage(%)	22.40	77.60	100.00

Fig. 14. SEM and EDS of Ni—P plating on AP plasma pretreated surface (O1P, 1 min): (a) magnification of 1000; (b) magnification of 5000; (c) magnification of 20,000; (d) EDS results.

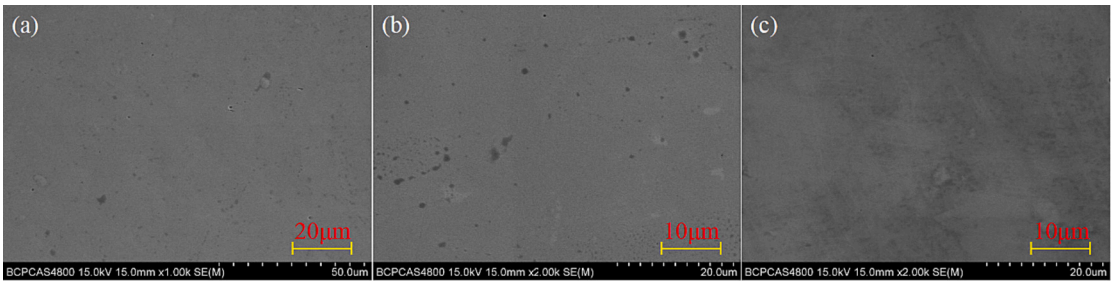

Fig. 15. SEM image of Ni—P plating on AP plasma pretreated surface: (a) O2P, 5 min; (b) O3P, 10 min; (c) O4P, 15 min.

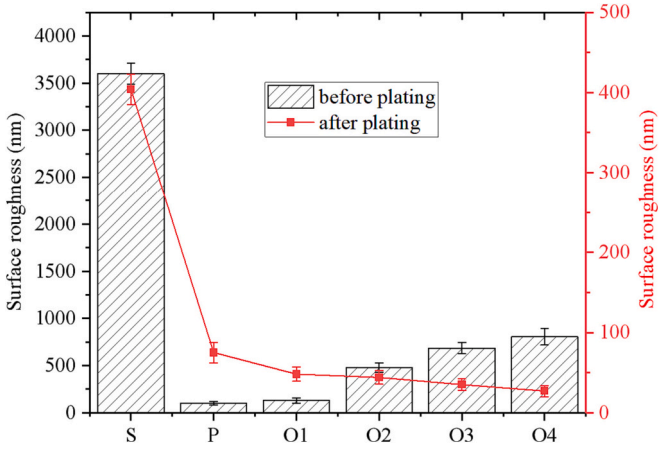

Fig. 16. Surface roughness before plating and after plating (S: sawing surface, P: polishing surface, O1: plasma treatment duration of 1 min, O2: plasma treatment duration of 5 min, O3: plasma treatment duration of 10 min, O4: plasma treatment duration of 15 min).

surfaces. Despite the increase in surface roughness due to longer AP plasma pretreatment, the Ni—P plated surface exhibits superior surface quality and achieves a roughness average (Ra) of approximately 27 nm.

The combined findings of the reduced surface roughness and improved surface topography through electroless Ni—P plating demonstrate the effectiveness of this process in enhancing the overall surface quality and smoothness of the Ni—P plated surface.

The hardness variation after Ni—P plating on different substate have been shown in Fig. 18. It is found that the hardness of the AP plasma enhanced Ni—P plating decrease a little bit, compared with the Ni—P plating produced by typical electroless Ni—P plating process on polished substrate. However, the effect of AP plasma pretreatment duration on the hardness of AP plasma enhanced Ni—P plating is not obvious considering the error of measurement results, as denoted O1, O2, O3 and O4.

The WCA measurements have been conducted after the Ni—P plating on different surface substrate, including the sawing substrate, polished substate and polished substrate with plasma processing duration of 1 min, 5 min, 10 min, 15 min as shown in Fig. 19. It can be observed that the WCA follow the trend of wettability of substrates without plasma surface modification, while the WCA of Ni—P plating on plasma enhanced Ni—P plating surface does not show too much difference and exhibiting hydrophobic property, as expected.

The phase composition of the Ni—P plating on sawing substrate, polished substrate and AP plasma pretreated substrates were analyzed by XRD pattern, as shown in Fig. 20. It is shown that the Ni—P plating on sawing substrate exhibits a broad peak of Ni (111) at 2θ of 45°. Narrow diffraction peaks, at 53° and 78.3°, correspond to crystallographic

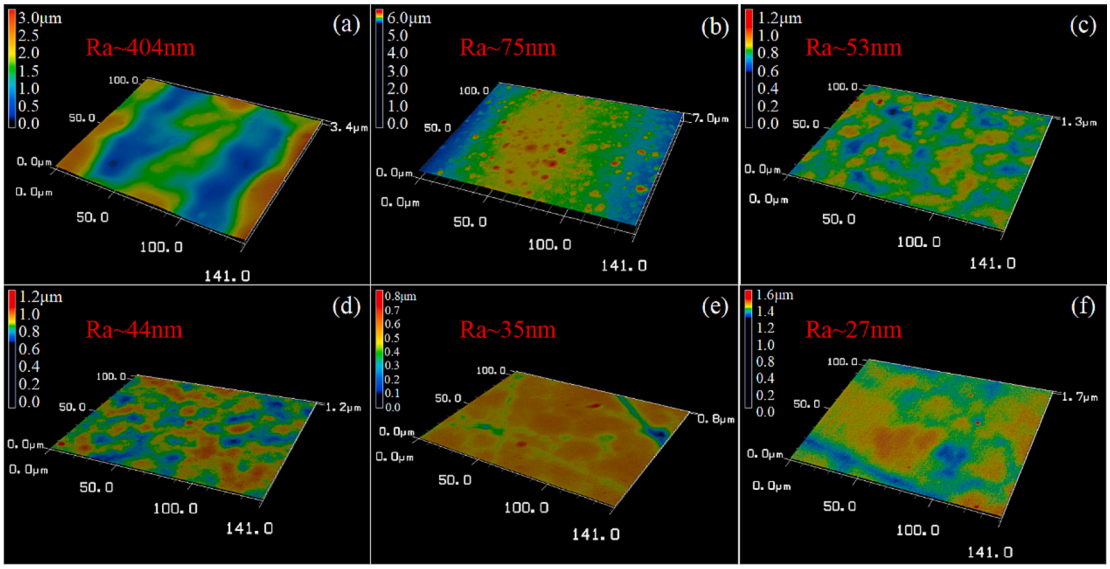

Fig. 17. Surface topography after Ni—P plating: (a) typical electroless Ni—P plating on sawing surface; (b) typical electroless Ni—P plating on polishing surface; (c) AP plasma enhanced Ni—P plating (O1P, 1 min); (d) AP plasma enhanced Ni—P plating (O2P, 5 min); (e) AP plasma enhanced Ni—P plating (O3P, 10 min); (f) AP plasma enhanced Ni—P plating (O4P, 15 min).

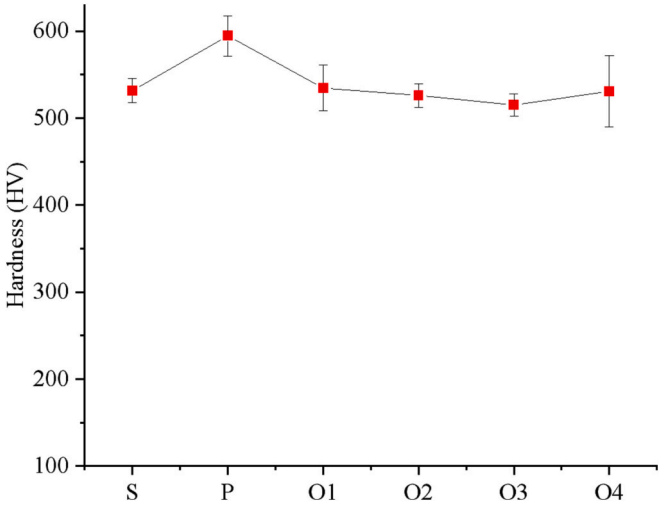

Fig. 18. Hardness measurement result (S: Sawing substrate, P: Polished substate, O1: polished substrate with plasma processing duration of 1 min, O2: polished substrate with plasma processing duration of 5 min, O3: polished substrate with plasma processing duration of 10 min, O4: polished substrate with plasma processing duration of 15 min).

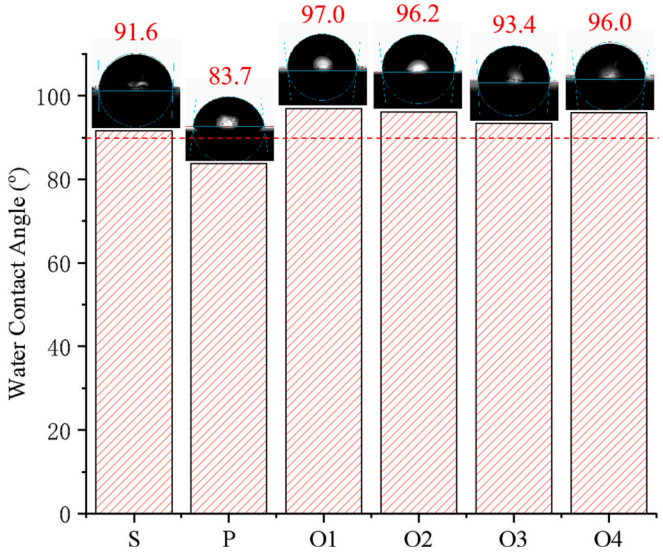

Fig. 19. Water contact angle results after Ni—P plating (S: Sawing substrate, P: Polished substate, O1: polished substrate with plasma processing duration of 1 min, O2: polished substrate with plasma processing duration of 5 min, O3: polished substrate with plasma processing duration of 10 min, O4: polished substrate with plasma processing duration of 15 min).

planes Ni (200), and Ni (220), respectively. The XRD pattern indicates Ni—P plating on sawing substrate contain a mixture of microcrystalline and amorphous phases [28]. Similarly, the XRD pattern of the Ni—P plating on polished substrate showcases prominent peaks approximately at 2θ of 45°, 53°, and 78.3°, corresponding to Ni (111), Ni (200), and Ni (220). However, new peaks emerge at 2θ of approximately 47.3°, 66.3°, and 74.7°, corresponding to crystallographic planes Ni_2P (210), Ni_2P (310), and Ni_2P (400), respectively. These additional peaks underscore the successful formation of Ni_2P phase in the polished sample. The phase transformation highlights the efficiency of the electroless Ni—P plating process in depositing Ni—P compound on the polished substrate, due to the improved uniformity and more favorable substrate for the formation of Ni2P phase with well-defined crystallographic orientations, compared with the sawing substrate [29].

The AP plasma enhanced Ni—P platings presents distinct peaks at 2θ of approximately 45° (Ni (111)) and 42.8°, 43.4°, 57.6°, 69.6°, and 73°, corresponding to crystallographic planes Ni_8P_3 (214), Ni_8P_3 (125), Ni_8P_3 (226), Ni_8P_3 (2122), and Ni (111), respectively, as illustrated in Fig. 20 (b). The intensities of the peaks are increased, and the widths of the peaks are narrower, indicating the phase transformation from amorphous to crystalline. The coexistence of metallic Ni and the formation of specific Ni—P compound, Ni_8P_3, resulting from the AP plasma enhanced Ni—P plating process, can be observed, which underscores the unique structural modifications achieved through plasma pretreatment. At the same time, the presence of Ni_8P_3 phase may exhibit better resistance to corrosion. Despite the improved surface quality, it is observed that O4 substrate after plasma duration of 15 min exhibits lower intensity of peaks and contain a higher proportion of amorphous phase, compared to the O1, O2, and O3 substrate. This is due to the higher roughness after

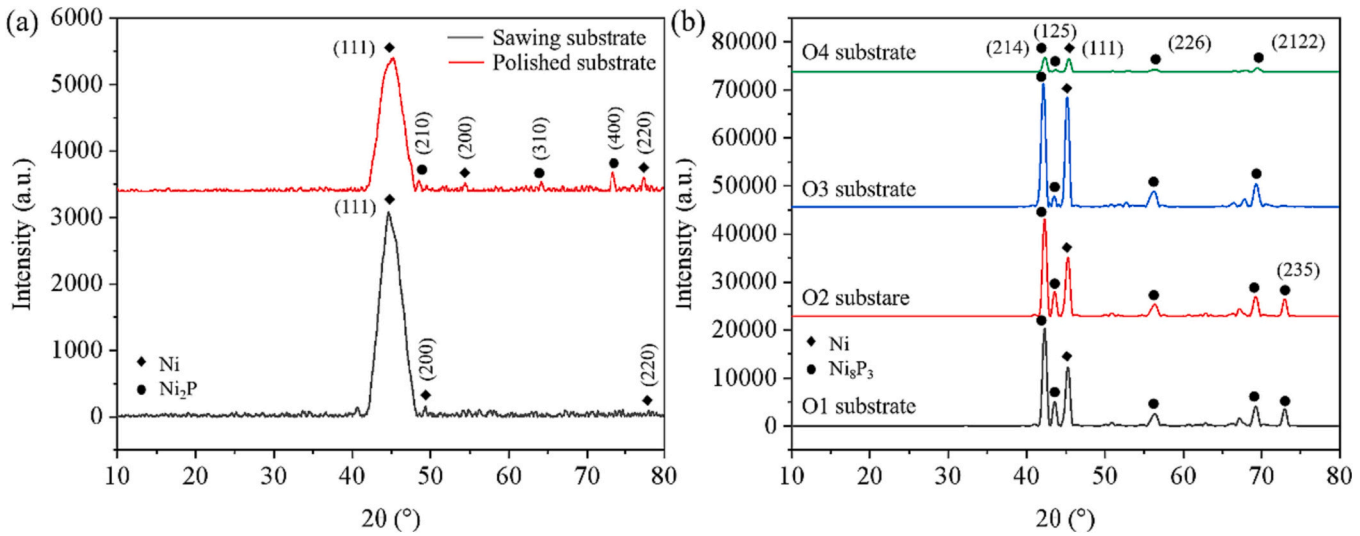

Fig. 20. XRD pattern after Ni—P plating: (a) S: Sawing substrate and P: Polished substate; (b) O1: polished substrate with plasma processing duration of 1 min, O2: polished substrate with plasma processing duration of 5 min, O3: polished substrate with plasma processing duration of 10 min, O4: polished substrate with plasma processing duration of 15 min.

AP plasma pretreatment, that can induce a higher degree of disorder in the surface of the substrate, promoting the formation of amorphous Ni—P [30].

To summarize, the surface roughness of the substrate is replicated to some extent in the plated surface, based on the results of typical electroless Ni—P plating process. Since the sawing surface has significant peaks and valleys, the plated Ni—P layer is likely to exhibit a higher roughness. Despite the improvement, the plating process generally follows the contours of the substrate, resulting in a plated surface with similar roughness characteristics. However, the increased surface roughness after AP plasma pretreatment can contribute to a smoothing effect during the plating process, for the polishing surface substrate. During AP plasma enhanced Ni—P plating, a rougher surface provides more surface area for the plating solution to spread and distribute evenly after AP plasma processing. The deposition of the Ni—P alloy can fill in some of the surface irregularities and create a more uniform surface. Additionally, plasma treatment activates the WC substrate's surface, generating reactive species that enhance the plating process. These activated sites promote nucleation and growth of the Ni—P layer, resulting in improved plating quality even on rougher surfaces. Along with increased surface energy, better distribution helps reduce overall Ni—P plating roughness.

Therefore, despite the formation of more amorphous Ni—P phase on the substrate with longer AP plasma pretreatment duration time and higher roughness, the dominant factors in AP plasma surface pretreatment for Ni—P plating are surface activation and surface energy improvement, which contribute to the desired surface roughness of the plated Ni—P layer. At the same time, the AP plasma enhanced Ni—P platings presents specific peaks, indicating phase transformation from amorphous to crystalline. To validate the adhesion improvement of AP plasma enhanced electroless Ni—P plating, the Rockwell-C indentation tests have been performed as follows.

3.4. AP plasma enhanced electroless Ni—P plating adhesion quality validation

As mentioned above, the Ni—P plating for sawing samples is incomplete and non-uniform on the WC substrate, it is not considered for adhesion test. Therefore, the Rockwell-C indentation tests have been performed under a load of 60 N on polished samples after typical electroless Ni—P plating and AP plasma enhanced Ni—P plating of different duration (O1P, 1 min; O2P, 5 min; O3P, 10 min; O4P, 15 min). The trace edges have been observed to evaluate the adhesion between the Ni—P plating and the WC substrate and the damage to the plating was compared with a defined adhesion strength quality. HF1-HF4 defines a sufficient adhesion whereas HF5 and HF6 represent an insufficient adhesion [31].

The indentation morphology results of the adhesion test on polished WC substrate are shown in Fig. 21. It is clearly shown that the indentation morphology after typical electroless Ni—P plating process is unacceptable failure with radical cracks. The Ni—P plating began to peel off and delamination happened at the same time, of which the enlarged location is shown in Fig. 21(b). According to VDI 3198 procedure, it can be concluded that the adhesion and bonding strength between Ni—P plating and WC substrate was the poor without AP plasma pretreatment and it is unacceptable for plating adhesion. This is due to the gas bubbles on the Ni—P plating surface, which arose from the hydrogen produced during the plating process that can diffuse into a WC substrate. If the gas bubble cannot be removed, the hydrogen can damage the near-surface region of the substrate, reducing adhesion by creating a brittle underlayer.

For comparison, Fig. 22 shows the indentation morphology results of the adhesion test between Ni—P plating and WC substrate on AP Plasma pre-treated WC substrate and the bonding quality have been shown greatly improved to acceptable level. The oval indentations left by the Rockwell indenter and the presence of radial cracks are evident. As shown in Fig. 22(a) and enlarged in 22(b), minor radial cracks and circumferential cracks within the indentations can be observed, indicating a fragile plating but with acceptable adhesion, which can be categorized as acceptable failure (HF3) for O1P. Fig. 22(c) shows the indentation morphology of AP plasma enhanced Ni—P plating with plasma duration of 5 min, O2P. Minor delamination can be observed in the vicinity of the indentation region. Additionally, circumferential cracks outside the indentations are observable in Fig. 22(d) on the AP plasma enhanced Ni—P plating with plasma duration of 10 min, O3P. O2P and O3P are therefore categorized as HF3 as well. While Fig. 22€ and (f) presents the adhesion test results for O4P substrates, revealing the presence of micro-spallation as a consequence of applied pressure and deformation, which is a cohesive failure, indicating a higher adhesion strength between the Ni—P plating and the WC substrate, compared to O1P, O2P, and O3P [32–34]. It is determined that the plating adhesion quality of all AP plasma pre-treated (O1P-O4P) are all acceptable and AP plasma pretreatment can enhance the mechanical locking between Ni—P plating and WC substrate. AP plasma pretreatment is

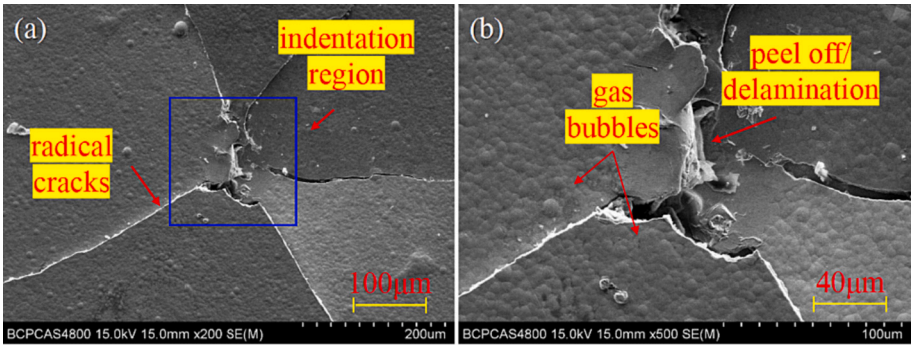

Fig. 21. Rockwell indentation morphology by SEM on typical electroless Ni—P plating on polishing surface without AP plasma pretreatment: (a) indentation region; (b) enlarged indentation region.

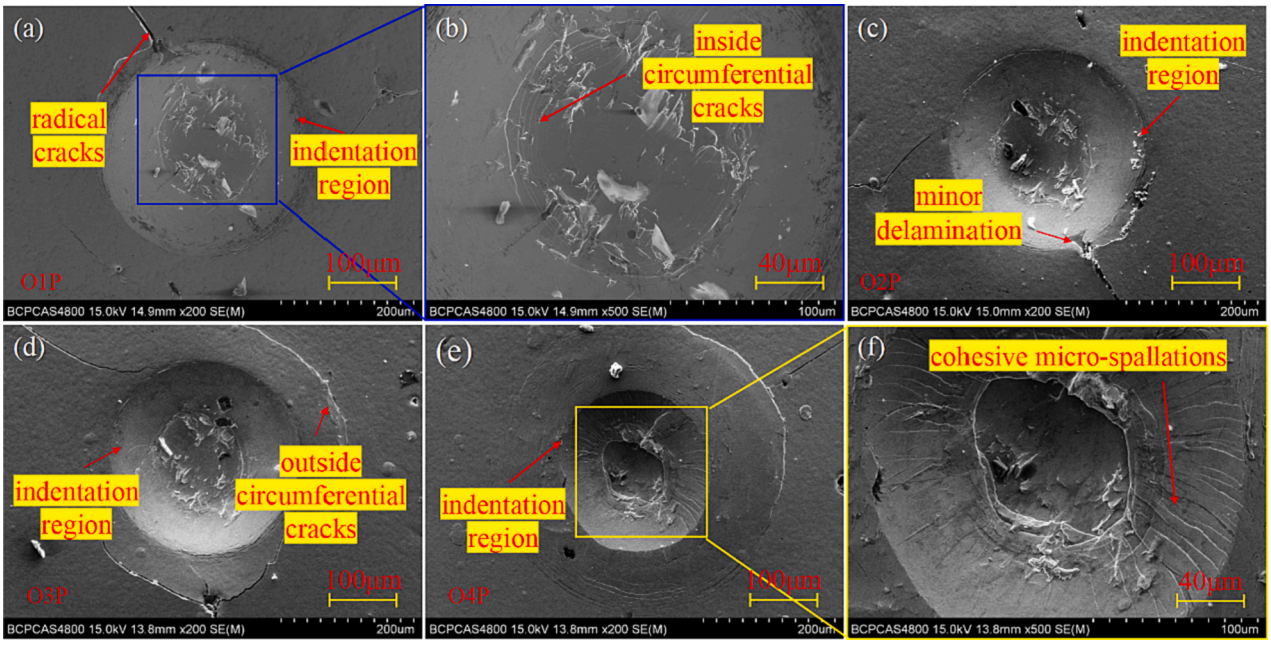

Fig. 22. Rockwell indentation morphology by SEM on AP plasma pretreated surface: (a) AP plasma enhanced Ni—P plating on O1P (1 min); (b) enlarged indentation region of O1P (1 min); (c) AP plasma enhanced Ni—P plating on O2P (5 min); (d) AP plasma enhanced Ni—P plating on O3P (10 min); (e) AP plasma enhanced Ni—P plating on O4P (15 min); (f) enlarged indentation region of O4P (15 min).

proved to be effective to improved adhesion between Ni—P plating and binderless WC substrate.

4. Conclusions

In this study, the effectiveness of ICP AP plasma surface processing as an alternative pretreatment technique for electroless Ni—P plating quality on binderless WC has been validated, contributing to the reduction of plating steps, time, smoothing of the plated Ni—P layer and improved adhesion between Ni—P plating and binderless WC substrate. The main conclusions are as follows:

(1) The study on the interaction mechanism between ICP AP plasma and binderless WC shows that AP plasma of short duration can lead to locally preferential oxidation along the grain boundaries and scratches. Anisotropic oxidation behavior can exhibit under certain experimental parameters. While longer processing can lead to isotropic oxidation behavior, where anisotropic or preferential oxidation becomes less prominent.

(2) During typical electroless Ni—P plating process, rough surface with irregularities provides localized areas with different surface orientations and growth conditions and can lead to variations in crystal growth, resulting in the development of distinct grain boundaries and grain-like structures. This may be due to the replication of substrate roughness during typical Ni—P plating process. The non-uniform deposition can result in areas with inadequate deposition and incomplete plating coverage.

(3) Despite the replication of substrate roughness during typical Ni—P plating process, the roughening by AP plasma pretreatment can also have a smoothing effect for Ni—P plating. AP plasma surface pretreatment can induce surface roughening and enhanced surface energy, during which the substrate can be effectively activated and cleaned. At the same time, the AP plasma enhanced Ni—P platings presents specific peaks, indicating phase transformation from amorphous to crystalline. These dominant factors contribute to the desired Ni—P plating quality and promoted adhesion quality between Ni—P plating and binderless WC.

This study can provide valuable insights into the feasibility and efficiency of using ICP AP plasma surface processing as an alternative pretreatment technique for high-quality electroless Ni—P plating on

binderless WC, which can have potential applications in PGM mold manufacturing.

CRediT authorship contribution statement

Weijia Guo: Conceptualization, Methodology, Writing – review & editing, Supervision, Funding acquisition. Muneeb Khan: Conceptualization, Methodology, Formal analysis, Investigation, Writing – original draft, review, editing. Tianfeng Zhou: Conceptualization, Methodology, Writing – review & editing, Supervision. Yupeng He: Conceptualization, Methodology. Yongjie Zhang: Conceptualization, Methodology. Peng Liu: Conceptualization, Methodology. Bin Zhao: Conceptualization, Methodology. Qian Yu: Conceptualization, Methodology. Xibin Wang: Formal analysis, Investigation. Hui Deng: Formal analysis, Investigation.

All authors have read and agreed to the published version of the manuscript.

Declaration of competing interest

The authors declare that they have no known competing financial interests or personal relationships that could have appeared to influence the work reported in this paper.

Data availability

Data will be made available on request.

Acknowledgement

This work was financially supported by the National Natural Science Foundation of China (52005040, 52205440, 52205441), the Beijing Municipal Natural Science Foundation (JQ20014), Science and Technology Major Project of Jiangxi Province (20212AAE01002).

References

[1] T. Zhou, Y. He, T. Wang, Z. Zhu, R. Xu, Q. Yu, B. Zhao, W. Zhao, P. Liu, X. Wang, A review of the techniques for the mold manufacturing of micro/nanostructures for precision glass molding, Int. J. Extreme Manuf. 3 (2021), 042002.
[2] L. Zhang, W. Liu, Precision glass molding: toward an optimal fabrication of optical lenses, Frontiers of, Mech. Eng. 12 (2017) 3–17.
[3] T. Zhou, Q. Zhou, J. Xie, X. Liu, X. Wang, H. Ruan, Elastic-viscoplasticity modeling of the thermo-mechanical behavior of chalcogenide glass for aspheric lens molding, Int. J. Appl. Glas. Sci. 9 (2018) 252–262.
[4] Z. Wang, J. Li, H. Qin, Y. Zhang, F. Zhang, Y. Su, Research of forming characteristic of precision glass molding, in: 8th International Symposium on Advanced Optical Manufacturing and Testing Technologies: Advanced Optical Manufacturing Technologies 9683, SPIE, 2016, pp. 366–371.
[5] G. Yan, F. Fang, Fabrication of optical freeform molds using slow tool servo with wheel normal grinding, CIRP Ann. 68 (2019) 341–344.
[6] M. Friedrichs, T. Grunwald, T. Bergs, Evaluation of mold materials for precision glass molding, in: Sixth European Seminar on Precision Optics Manufacturing 11171, SPIE, 2019, pp. 60–65.
[7] H. Zhao, A.K. Gain, Z. Li, L. Zhang, Wear of mold surfaces: interfacial adhesion in precision glass molding, Wear 04847 (2023).
[8] K. Georgiadis, The Failure Mechanisms of Coated Precision Glass Molding Tools, Apprimus Wissenschaftsverlag, 2015.
[9] A. Brenner, G.E. Riddell, Nickel plating on steel by chemical reduction, Plat. Surf. Finish. 85 (1998) 54–55.
[10] G.O. Mallory, J.B. Hajdu, Electroless Plating: Fundamentals and Applications, William Andrew, 1990.
[11] S. Zhang, K. Han, L. Cheng, The effect of SiC particles added in electroless Ni–P plating solution on the properties of composite coatings, Surf. Coat. Technol. 202 (2008) 2807–2812.
[12] M. Jafari, M.H. Enayati, M. Salehi, S.M. Nahvi, C.G. Park, Microstructural and mechanical characterizations of a novel HVOF-sprayed WC-co coating deposited from electroless Ni–P coated WC-12Co powders, Mater. Sci. Eng. A 578 (2013) 46–53.
[13] G. Di Egidio, C. Martini, L. Ceschini, A. Morri, Influence of electroless nickel—DLC (diamond-like carbon) multilayer coating on the mechanical performance of the heat-treated AlSi10Mg alloy produced by powder bed fusion-laser beam, Materials 16 (2023) 3313.
[14] K.H. Krishnan, S. John, K.N. Srinivasan, J. Praveen, M. Ganesan, P.M. Kavimani, An overall aspect of electroless Ni-P depositions—a review article, Metall. Mater. Trans. A 37 (2006) 1917–1926.
[15] S. Kundu, P. Sahoo, S.K. Das, Optimization studies on electroless nickel coatings: a review, Int. J. Manuf. Mater. Mech. Eng. 4 (2014) 1–25.
[16] J. Xu, T. D. Hall, C. Crowley, S. Snyder, B. Skinn, M. E. Inman, E. J. Taylor, A Novel Pretreatment Process for Direct Electrodeposition onto Aluminum Alloys.
[17] H.B. Lee, K.L. Chen, J.W. Su, C.Y. Lee, The use of surfactants and supercritical CO_2 assisted processes in the electroless nickel plating of printed circuit board with blind via, Mater. Chem. Phys. 241 (2020), 122418.
[18] W.P. Wu, J.J. Jiang, Effect of plating temperature on electroless amorphous Ni–P film on Si wafers in an alkaline bath solution, Appl. Nanosci. 7 (2017) 325–333.
[19] Q. Yu, T. Zhou, Y. He, P. Liu, X. Wang, Y. Jiang, J. Yan, Annealed high-phosphorus electroless Ni–P coatings for producing molds for precision glass molding, Mater. Chem. Phys. 262 (2021), 124297.
[20] S. Dabees, S. Mirzaei, P. Kaspar, V. Holcman, D. Sobola, Characterization and evaluation of engineered coating techniques for different cutting tools, Materials 15 (2022) 5633.
[21] H. Ma, F. Tian, D. Li, Q. Guo, Study on the nano-composite electroless coating of Ni–P/Ag, J. Alloys Compd. 474 (2009) 264–267.
[22] S.M.A. Shibli, B. Jabeera, R.I. Anupama, Incorporation of nano zinc oxide for improvement of electroless nickel plating, Appl. Surf. Sci. 253 (2006) 1644–1648.
[23] N.K. Shrestha, D.B. Hamal, T. Saji, Composite plating of Ni-P-Al_2O_3 in two steps and its anti-wear performance, Surf. Coat. Technol. 183 (2003) 247–253.
[24] W. Song, D.Y. Shan, E.H. Han, High corrosion resistance of electroless composite plating coatings on AZ91D magnesium alloys, Electrochim. Acta 53 (2008) 2135.
[25] Y. Zhang, L. Zhang, K. Chen, D. Liu, D. Lu, H. Deng, Rapid subsurface damage detection of SiC using inductivity coupled plasma, Int. J. Extreme Manuf. 3 (2021), 035202.
[26] A.Ya. Pak, I.I. Shanenkov, G.Y. Mamontov, A.I. Kokorina, Vacuumless synthesis of tungsten carbide in a self-shielding atmospheric plasma of DC arc discharge, Int. J. Refract. Met. Hard Mater. 93 (2020), 105343.
[27] R. Libanori, D. Carnelli, N. Rothfuchs, M.R. Binelli, M. Zanini, L. Nicoleau, B. Feichtenschlager, G. Albrecht, A.R. Studart, Composites reinforced via mechanical interlocking of surface-roughened microplatelets within ductile and brittle matrices, Bioinspiration Biomimetics 11 (2016) 036004.
[28] L. Yang, J. Li, Y. Zheng, Y.W. Jiang, M. Zhang, Electroless Ni-P plating with molybdate pretreatment on Mg-8Li alloy, J. Alloys Compd. 467 (2009) 562–566.
[29] J. Deng, K. Li, J. Fu, B. Liu, H. Jiang, Preparation and properties of textured Ni–W coatings electrodeposited on the steel surface from a pyrophosphate bath, Coatings 13 (9) (2023) 1519.
[30] A. Kumar, A.K. Suhang, A.S. Singh, Deposition and characterization of amorphous electroless Ni-Co-P alloy thin film for ULSI application, Surf. Coat. Technol. 1 (3) (2014), 035007, https://doi.org/10.1088/2053-1591/1/3/035007.
[31] X. Zhang, X. Tian, Z. Zhao, J. Gao, Yan Zhou, P. Gao, Y. Guo, Z. Lv, Evaluation of the adhesion and failure mechanism of the hard CrN coatings on different substrates, Surf. Coat. Technol. 364 (2019) 135–143.
[32] N. Vidakis, A. Antoniadis, N. Bilalis, The VDI 3198 indentation test evaluation of a reliable qualitative control for layered compounds, J. Mater. Process. Technol. 143 (2003) 481–485.
[33] R. Souza, A. Sinatora, G. Mustoe, J. Moore, Numerical and experimental study of the circular cracks observed at the contact edges of the indentations of coated systems with soft substrates, Wear 251 (2001) 1337–1346.
[34] A. Gilewicz, R. Jedrzejewski, P. Myslinski, B. Warcholinski, Structure, morphology, and mechanical properties of AlCrN coatings deposited by cathodic arc evaporation, J. Mater. Eng. Perform. 28 (2019) 1522–1531.